

IMPLEMENTATION OF A TUNED MASS DAMPER: A PHYSICAL MODEL APPROACH

Duque^{a,b}, Edwin; Inaudi, José^{c,d}

^aEstudiante de Doctorado, Facultad de Ciencias Exactas Físicas y Naturales, Universidad Nacional de Córdoba, Argentina

epduque@utpl.edu.ec

^bDepartamento de Ingeniería Civil, Universidad Técnica de Loja, Ecuador epduque@utpl.edu.ec

°Facultad de Ingeniería, Universidad Católica de Córdoba, Argentina inaudijose@gmail.com

^dFacultad de Ciencias Exactas Físicas y Naturales, Universidad Nacional de Córdoba, Argentina

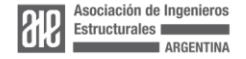
jose.antonio.inaudi@unc.edu.ar

RESUMEN

Este documento presenta la implementación de un modelo físico para analizar la respuesta dinámica de un sistema estructura-amortiguador de masa sintonizada (AMS) en modelo de estructura tipo marco plano. Se describen los procesos de diseño, fabricación y caracterización de componentes, así como su montaje e integración en el sistema estructural. La validación del modelo se realizó comparando la respuesta experimental con predicciones teóricas, mostrando una correlación adecuada. Además, se evaluó la efectividad del AMS en la reducción de vibraciones, evidenciando una disminución significativa en la respuesta dinámica de la estructura equipada con el AMS en comparación con la estructura sin amortiguador. Estos resultados muestran la precisión del modelo físico y su utilidad para estudios futuros de optimización del AMS.

ABSTRACT

This paper presents the implementation of a physical model to analyze the dynamic response of a structure-Tuned Mass Damper (TMD) system in a shear frame model. The design, fabrication, and component characterization processes are described, along with their assembly and integration into the structural system. The validation of the model was performed by comparing the experimental response with theoretical predictions, showing a good correlation. Additionally, the effectiveness of the TMD in vibration reduction was evaluated, demonstrating a significant decrease in the dynamic response of the structure equipped with the TMD compared to the structure without the mass damper. These results highlight the accuracy of the physical model and its utility for future studies aimed at optimizing TMD performance.





INTRODUCCIÓN

Tuned Mass Dampers (TMDs) are devices widely used in structural engineering to mitigate vibrations induced by dynamic loads, such as wind or earthquakes. Their operation is based on absorbing the vibrational energy of a structure through an additional mass-spring-damper system. TMDs can be studied from different approaches, including theoretical analysis, numerical simulations, and experimental studies using physical models.

In the theoretical domain, numerous studies have developed mathematical models that describe the dynamic behavior of TMDs, such as the works of (Den Hartog, 1956) and (Warburton, 1982), which laid the foundations for optimizing these devices. Numerical simulation has also been extensively used, allowing the analysis of complex systems under various conditions, as seen in the studies by (Rana & Soong, 1998), (Tsai & Lin, 1993), (Duque et al., 2015) y (García et al., 2021), who employed computational models to evaluate the effectiveness of TMDs in various structures and with different TMD configurations.

However, physical models offer a significant advantage by visually representing the system's behavior under real conditions. These models allow the validation of theories and simulations and the observation of phenomena that numerical methods might not capture. Research such as that by (Carmona et al., 2017; Dekemele et al., 2020; Jiang et al., 2019; Roffel et al., 2010; J. Wang et al., 2020; L. Wang et al., 2023) have demonstrated the efficacy of TMDs through scale model tests, highlighting the importance of experimental studies in the detailed understanding of these devices' behavior.

In this context, the present work focuses on designing, implementing, and validating a physical TMD model mounted on a shear-frame experimental model. The main objective is to demonstrate the process of fabricating the physical model, ensuring its fidelity in representing the theoretical system. This paper details the necessary steps for constructing the physical model, from the design, characterization, and fabrication of the components to their integration into the structural system. Although the detailed analysis of the TMD's dynamic behavior will be addressed in future research, this work lays a solid foundation for such experimental evaluations, providing a clear understanding of the physical model development process.

The document is structured into five sections. The first section outlines the theoretical model and the design parameters required for the construction of the physical model. The second section focuses on the conceptualization of the physical model, detailing the structural system, its components, and the necessary formulation for the design of each element, including the construction drawings for subsequent implementation in the physical model. The third section provides a detailed account of the assembly process conducted in a mechanical workshop, covering the entire construction procedure. The fourth section presents the experimental results, comparing the dynamic response of the structure with and without the TMD. Finally,





the fifth section discusses the study's conclusions and proposes directions for future research.

MODELO TEORICO

Consider the dynamic system shown in Figure 1, comprising several degrees of freedom. This system consists of two main elements: (i) a primary mass, m_s , connected to the ground via a linear spring with stiffness k_s and viscous damping c_s , and (ii) a Tuned Mass Damper (TMD) composed of three single-degree-of-freedom (3-DOF) subsystems, each consisting of a secondary mass $(m_{TMD1}, m_{TMD2}, m_{TMD3})$ connected to the primary mass through springs with stiffness $k_{TMD1}, k_{TMD2}, k_{TMD3}$ and damping $c_{TMD1}, c_{TMD2}, c_{TMD3}$.

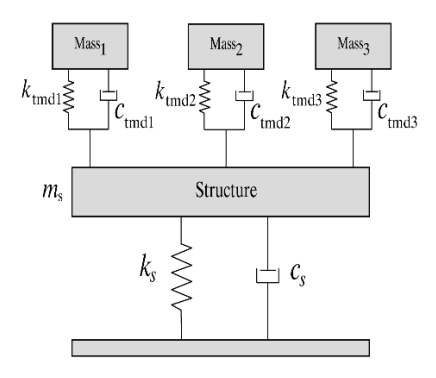


Figure 1. Theoretical model for a multi-degree-of-freedom dynamic system. The first component is the primary structure, while the second is a tuned mass damper (TMD).

The design parameters used for constructing the physical model, presented in Table 1, were selected to ensure an adequate representation of the dynamic behavior of the system under study, considering a period of 0.811 seconds, corresponding to a slender building, and a mass ratio between the primary structure and the TMD of $\mu = 9.82\%$. The values shown in the table represent the total values for the TMD; each subsystem has one-third of the defined values.

Parameter	Symbol	Value	Units
Mass of the primary structure	$m_{\scriptscriptstyle S}$	9.5545	Kg
Stiffness of the primary structure	k_s	469	N/m
Damping of the primary structure	c_s	0.388	N*s/m
Mass of the TMD	m_{TMD}	0.97269	Kg
Stiffness of the TMD	k_{TMD}	53	N/m
Damping of the TMD	c_{TMD}	2.17	N*s/m





DESCRIPTION OF THE PHYSICAL MODEL

Design of the Primary Structure

The primary structure is a single-story shear-frame made of steel and aluminum (See Figure 2). Four elements stand out in the chosen system: the slab, walls, connections, and support base. These components have been designed to form a modular system that can be used to build more complex models if necessary.

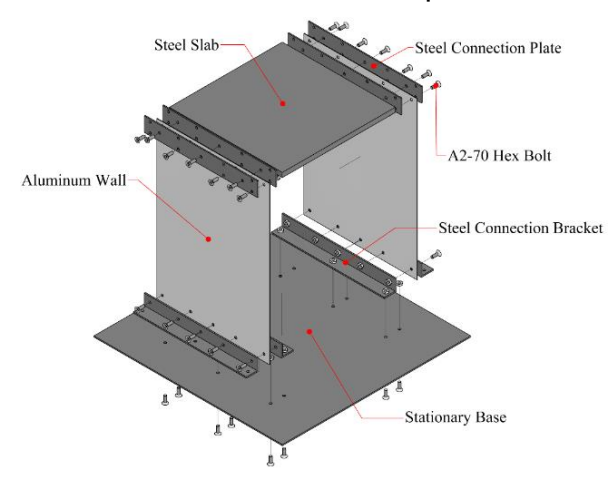


Figure 2. Primary structure conceived as a single-story shear-frame model.

For modeling purposes, the structural system can be considered a mass-springdamper system as long as the mass at the top is considerably more significant than the mass of the walls, and these are ideally fixed both at the base and the top. Since the idealized shear frame meets these restrictions, dynamic parameters, such as mass, stiffness, and, thus, natural frequency, can be calculated using the relevant equations for each case.

The mass of the system, m_{eq} , is composed of the sum of the slab mass, the connection plate mass, and one-third of the total wall mass, as specified in Eq. (1).

$$m_{eq} = m_{slab} + m_{plates} + \frac{1}{3}m_{walls} \tag{1}$$

Where:

 m_{slab} = slab mass, m_{plates} = connection plate mass, m_{walls} = wall mass.

Similarly, the lateral stiffness of a wall in the shear frame can be evaluated using Eq. (2).

$$k_{eq} = \frac{Et^3w}{L^3} \tag{2}$$

Where:

E = Modulus of elasticity, t = Wall thickness, w = Wall width, L = Length. Organiza:





The natural frequency and period of the structural system are calculated using Eqs. (3) and (4), respectively, based on the previously defined parameters:

$$f = \frac{\sqrt{\frac{k_{eq}}{m_{eq}}}}{2\pi} \tag{3}$$

$$T = \frac{1}{f} \tag{4}$$

Design of the TMD

The tuned mass damper consists of three parallel single-degree-of-freedom (3-DOF) systems, each with identical dynamic parameters. Each of these systems is composed of four main elements: the concentrated mass, the linear spring, the viscous damper, and the sliding systems (See Figure 3). Before implementing each element, they must be carefully designed, and the required expressions are described below.

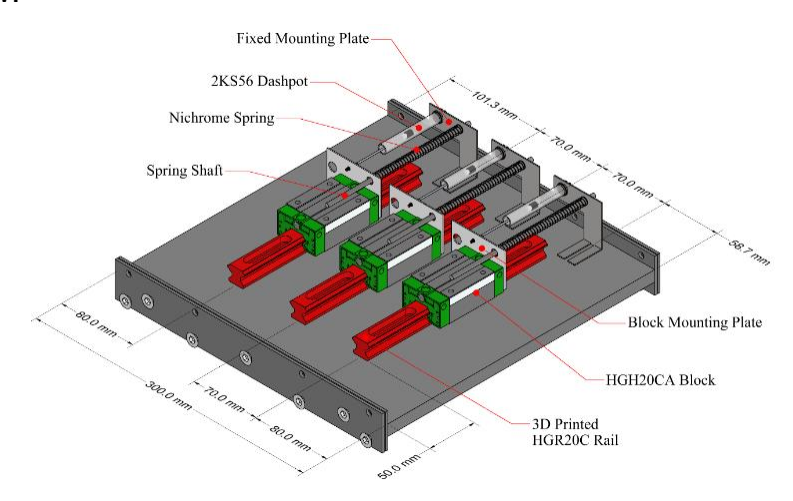
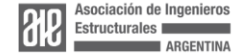


Figure 3. Tuned mass damper (TMD), consisting of three single-degree-of-freedom (3-DOF) systems placed in parallel with identical dynamic parameters.

Traditionally, prefabricated helical springs with predefined stiffness characteristics are used to obtain the stiffness of the TMD. However, since the global stiffness must be 53 N/m, and due to the complexity of finding a spring that provides exactly this stiffness, and considering that this stiffness must be distributed among the three elements of the damped system, meaning each spring must provide a stiffness of 17.67 N/m, it was decided to design and manufacture customized helical springs. For this purpose, Eq.(5), which describes the relationship between the spring stiffness and its physical and mechanical characteristics, was used:





$$k_{r=} \frac{Gd^4}{8D^3N} \tag{5}$$

Where:

G: Shear modulus of the wire, d: Wire diameter, D: Mean spring diameter, and N: Number of spring coils.

The viscous damping of the TMD was generated using Dashpot 2KS56 air dampers, which offer a damping range between 0 N/(mm/s) and 0.088 N/(mm/s). The required damping value can be adjusted through a needle valve located at the bottom of the Dashpot, calibrated to directly obtain the desired damping value (2.17 N/mm). Although this process does not require a specific mathematical formulation, it is necessary to experimentally determine the precise valve opening angle for the Dashpot to provide the desired damping.

Similarly, the sliding systems used consisted of linear rails with internal bearings that allowed the linear displacement of the masses (See Figure. 4). Although the bearings are characterized by generating low friction force (F_f) , it is essential to quantify the friction level between the mass and the rail to evaluate its possible influence on the system. To do this, the horizontal force required to move the block along the rail and the normal force due to the block's weight are considered, as shown in Eq(6).

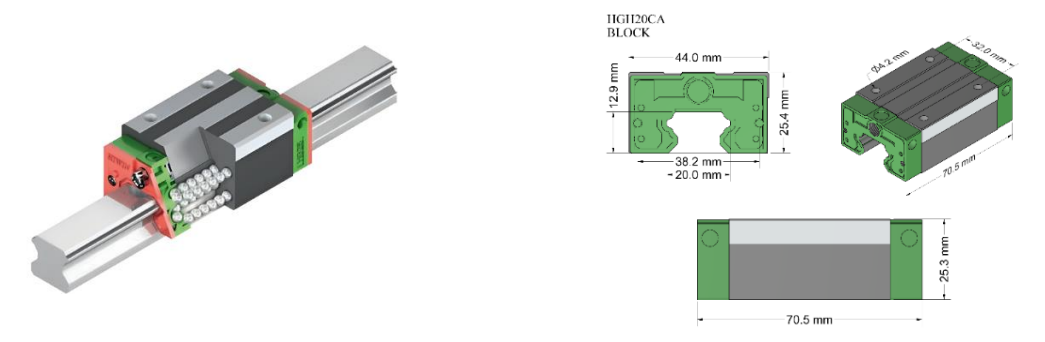


Figure. 4. Rail-block system consisting of a linear rail, block, and internal bearings that allow the linear displacement of the masses.

$$\mu = \frac{F}{W_b} \tag{6}$$

Where:

F: Horizontal force required to move the block, W_b : force due to the block's weight



Both the evaluation of the dry friction coefficient (μ) and the determination of the precise valve opening angle for the Dashpot were conducted experimentally through the procedure described in the following section.

Components of the Primary Structure and TMD

The geometry and configuration of the primary structure and TMD components were determined using Eqs. (1) al (6). The material must be defined, and the target design values shown in Table 1 must be applied. The elements of the global structure-TMD system used in constructing the physical model are described below.

Slab

The slab is made of carbon steel, chosen for its high mass concentration. It has a thickness of 12 mm and dimensions of 300 mm in length and 300 mm in width, with 6 threaded inserts for bolts, each with a diameter of 6 mm. Additionally, threaded inserts were integrated into the connection system, as illustrated in Figure 5a. This measure was implemented to strengthen the connection between elements, improving the structural efficiency and overall resistance.

Connections

The connections, shown in Figure 5b, have two main functions: to join the walls with the slab and to anchor the structural system to the base. These connections are made of carbon steel using 1 ¼" L angles, with five holes distributed along their length to allow the passage of bolts used in the system assembly. The connections are 300 mm long, which is necessary for anchoring them to the slab and support base.

Walls

The walls, shown in Figure 5c, are made of aluminum (E = 69 GPa). Each wall has dimensions of 300 mm in width, 417 mm in height, and 1 mm in thickness, which provides the expected stiffness for the primary structure of 544 N/m, calculated from Eq (2). Additionally, they feature holes distributed across their width, as shown in Figure 5c.

Support Base

The support base is essential for assembling the structure, facilitating its installation on a testing system or simply for its placement on the floor. The geometric configuration of this element is shown in Figure 5d, particularly highlighting the inserts designed for assembly with the connections.



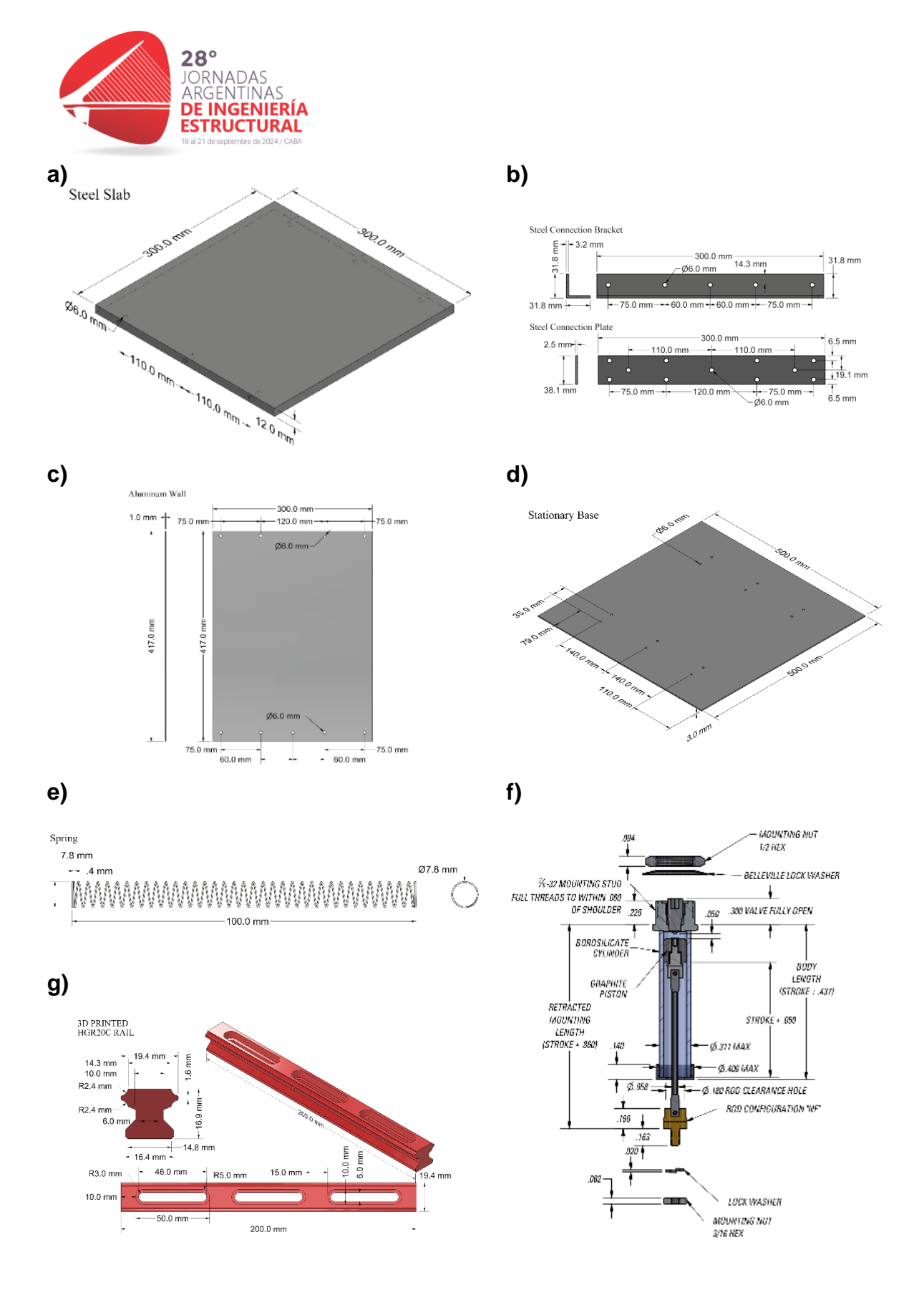


Figure 5 Components of the primary structure and TMD. a) Slab, b) connections, c) walls, d) support base, e) Nichrome spring, f) air-type piston dampers, g) sliding systems.



Nichrome Spring

The Nichrome spring was designed using Eq (5), employing 0.4 mm diameter Nichrome wire as the primary material. The adopted shear modulus was 82 GPa, with an average spring diameter of 7.4 mm (the difference between the turn diameter of 7.8 mm and the wire diameter) and 36 turns (N). Based on this data, the theoretical stiffness constant obtained for each spring was 17.9 N/m. Considering that the target stiffness was 17.67 N/m, the difference was deemed acceptable for the model's purposes. The geometry of the spring is shown in Figure 5e.

As previously mentioned, the springs needed to be constructed, unlike the elements described earlier, which could be directly acquired from manufacturers. Their fabrication was a meticulous process (See Figure 6a). This process began with winding the Nichrome wire to form the spring. Once formed, the spring was connected to a power source to heat it and set its shape. During heating, current and voltage were monitored to ensure uniform thermal treatment. After treatment, the spring was cooled and visually inspected to ensure it maintained the desired stiffness.

The construction of the springs concluded with their validation to ensure each achieved the desired stiffness. For this purpose, a tensile test was performed using the SHIMADZU AGS-X 10 kN STD E100V testing machine (See Figure 6b). The test involved subjecting the springs to tension until reaching a controlled displacement of 50 mm. This procedure allowed for determining the forces generated throughout the entire range of motion, which were recorded and subsequently analyzed. Figure 6c shows the results obtained for three springs, where the approximate experimental stiffness of 17.6 N/m, calculated as the ratio of force to displacement, is similar to the theoretical stiffness with which they were designed (17.9 N/m) as well as the target stiffness (17.67 N/m).

The observed stiffness variations may be due to differences in the technical specifications of the materials, possible manufacturing errors, or the sensitivity of the testing equipment used. However, as will be seen later, these differences are irrelevant to the overall system behavior and fall within an acceptable range.

Air-Type Piston Dampers

As previously mentioned, the dampers used in the model's fabrication are Dashpot 2KS56, whose components are schematically illustrated in Figure 5f. To ensure that the damping provided by the dampers is adequate, and given that the manufacturer does not specify the valve opening calibration concerning the damping coefficient, it was necessary to characterize the Dashpots' behavior according to the valve opening degree to set the damping to the desired value.





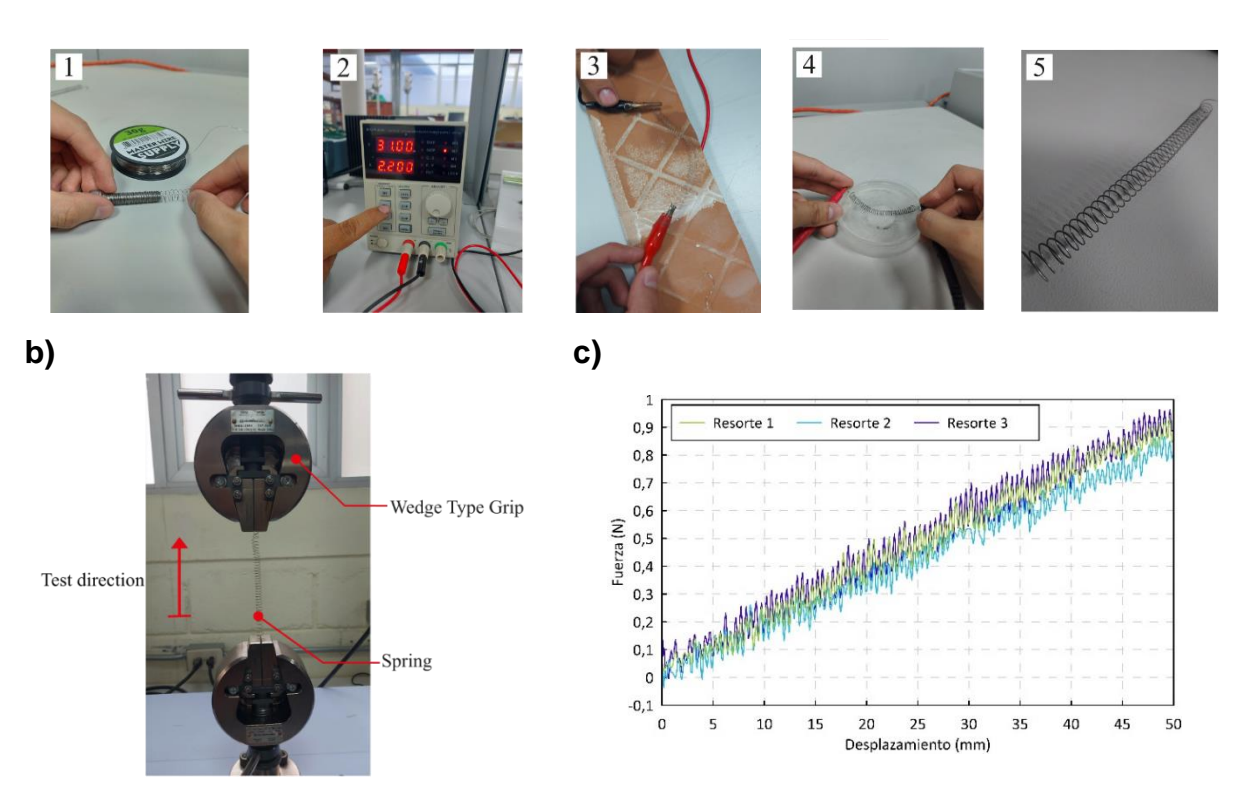


Figure 6. Construction process and stiffness validation of the spring constants. a) Construction process of a spring summarized in five main phases. b) Tensile test for estimating the axial stiffness of a spring. c) Force and displacement results obtained from the tensile test.

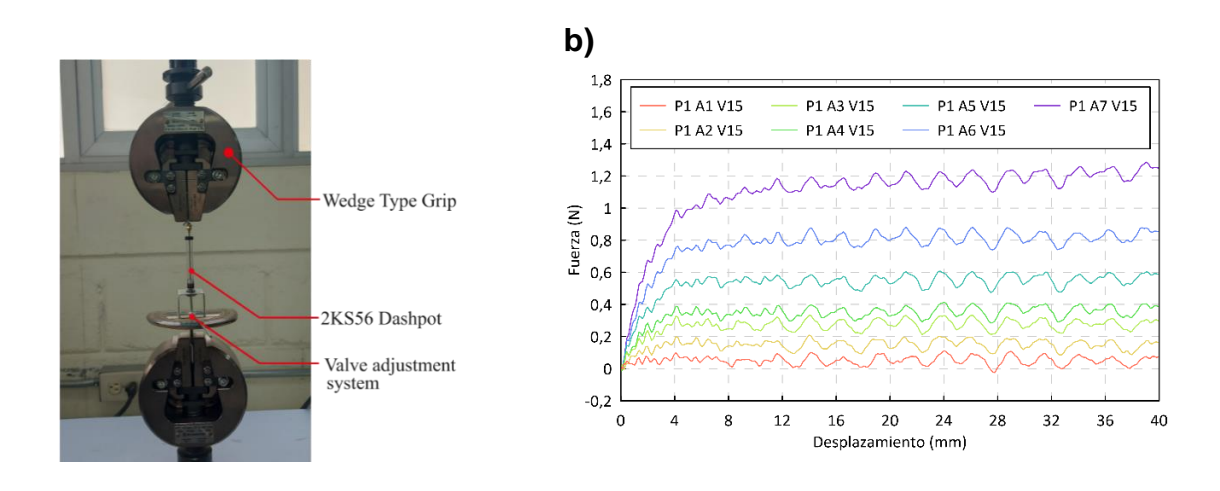


Figure 7. Dashpot characterization test. a) Positioning of the Dashpot in the SHIMADZU AGS-X 10 kN STD E100V machine to apply a tensile force. b) Force-displacement relationship obtained when testing Dashpot 1 for seven different valve openings (215°, 175°, 135°, 125°, 115°, 105°, 95°) and a constant speed of 15 mm/s.





To achieve this, each Dashpot underwent a tensile test. This test involved positioning the Dashpots vertically between the jaws of the testing machine, as shown in Figure 7a, and pulling the piston rod over a distance of 40 mm while recording the force generated by the Dashpot throughout the entire stroke. This test was conducted at three speeds: 5, 10, and 15 mm/s, with a total of seven valve opening degrees (215°, 175°, 135°, 125°, 115°, 105°, 95°). Three repetitions were performed for each condition (E1, E2, E3) to ensure the reliability of the results, obtaining a total of 189 tests.

Although results were obtained for all possible combinations, Figure 7b shows, as an example, the test results conducted with Dashpot 1 (P1), where the force-displacement relationship for the seven described openings at a speed of 15 mm/s can be observed.

Sliding Systems.

The sliding system and the block were acquired from the Hiwin brand, with commercial codes HGH20CA for the block and HGR20 for the rail, respectively. Although the bearing system provides low friction, upon inspection, it was considered inadequate for the scale of the physical model. Additionally, the original system includes a preload mechanism designed to keep the mass fixed until a preassigned preload value is applied. This feature is desired in devices where a mass of larger proportions than that of this study needs to be mobilized.

Therefore, it was decided to design and subsequently 3D print rails that do not incorporate the preload mechanism and minimize friction between the TMD mass and the supporting rail. The general configuration of the designed rails was based on the originals (HGR20C), paying particular attention to not affecting the bearing seating system, using resin as the primary material. The geometry of the rails is shown in Figure 5g.

To evaluate the friction generated between the designed rail and the block (HGH20CA), the SHIMADZU AGS-X 10 kN STD E100V machine was adapted to record the horizontal force opposing the block's movement and, consequently, the friction, as schematically shown in Figure 8a. The test consisted of positioning the rail-block system on the base and then conducting traction tests, recording the force required to move the system as a whole, as shown in Figure 8b. Considering the recorded force, the block's weight (324.23 g), and applying Eq. (6), the friction coefficient was obtained, as shown in Figure 8c. This figure presents the friction for two rails along their length (200 mm) and for three different load application speeds: 5, 10, and 15 mm/s. The test results show that the friction coefficient is not sensitive to load application speeds and that the friction generated between the sliding system and the block is approximately $\mu=0.03$.





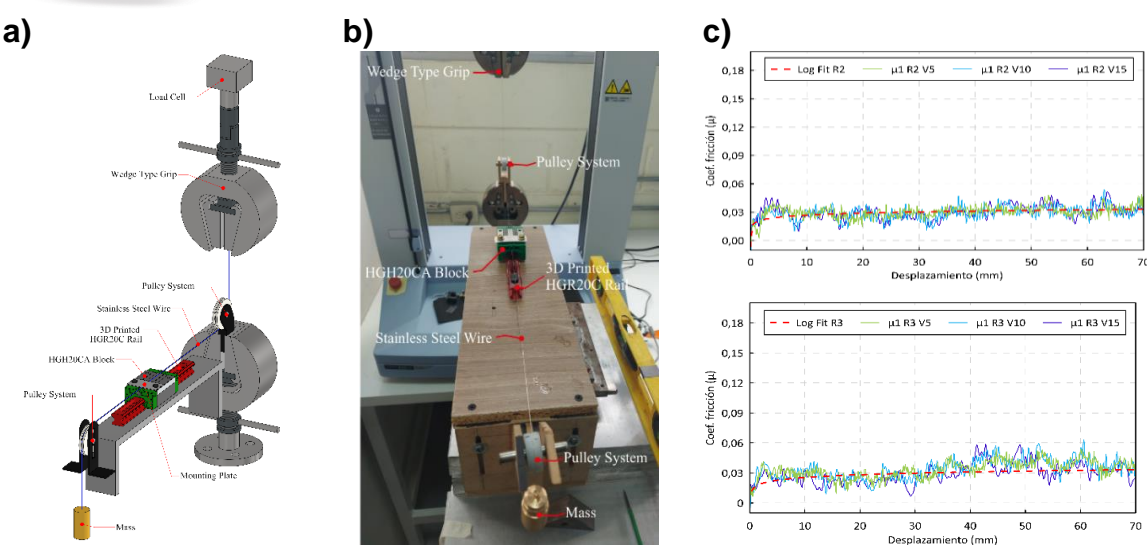


Figure 8. Friction test conducted on the rail-block system. a) Schematic representation of the adaptation made to the SHIMADZU AGS-X 10 kN STD E100V machine to perform the test. b) Testing process carried out to estimate the friction. c) Results of the friction test.

STRUCTURAL SYSTEM ASSEMBLY

The construction process of the complete system, including both the primary structure and the Tuned Mass Damper (TMD), was developed in several carefully planned phases, ensuring precision at each stage to guarantee the stability and functionality of the physical model.

Primary Structure Assembly

The assembly of the primary structure was carried out following a specific chronology to ensure the correct alignment and fastening of all components (See Figure 9). The process began with attaching the slab to the upper connections through welding. This initial step ensured a solid and resistant connection between the slab and the connections, which would support the walls. Next, the support base was attached to the lower connections, also through welding, ensuring structural integrity from the base. Finally, the walls were mounted on the base and slab using rivets. The aluminum walls were carefully aligned and fixed to ensure a secure and stable connection.

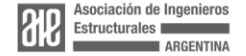














Figure 9. Primary structure assembly process.

Tuned Mass Damper (TMD) Assembly

The assembly of the TMD was carried out in four stages (See Figure 10). First, the linear rails were installed on the slab using bolts, ensuring proper alignment to allow for uniform mass sliding. Then, the plates that will serve as bases for the spring and damper were positioned, fastening them precisely to ensure efficient installation. Subsequently, the sliding block was inserted onto the rails, ensuring that the internal bearings that facilitate movement were unobstructed. Finally, the helical spring and dashpot air damper were placed on the plates. These components were carefully adjusted to provide the necessary stiffness and damping, thus completing the TMD assembly. This process, conducted with precision, ensures optimal system integration with the primary structure.









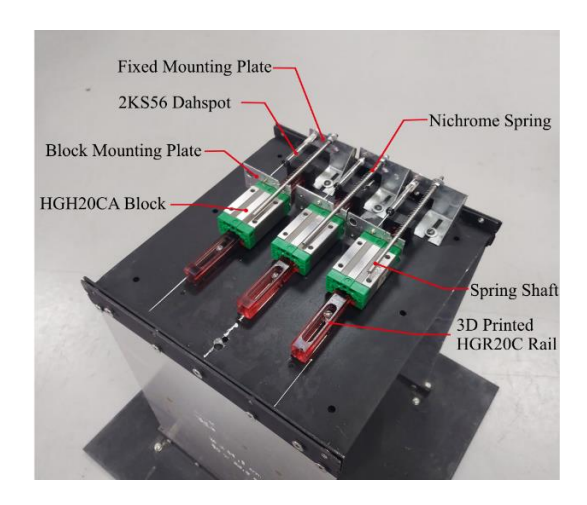


Figure 10. Tuned Mass Damper (TMD) assembly process





DYNAMIC RESPONSE OF THE PHYSICAL MODEL

This section presents the dynamic response of the physical model, encompassing both the main structure and the system combined with the Tuned Mass Damper (TMD) under initial conditions. The objective is to validate the dynamic behavior of the model, including its characteristic parameters.

Initially, a free vibration test was conducted on the structure without the TMD, applying displacement and velocity initial conditions ($x_0 = 0.02m$ and $v_0 = 0\,m/s$). The time response was recorded using low-cost accelerometers designed and constructed at the Structures Laboratory of UTPL-Ecuador. Simultaneously, the theoretical response of the system was calculated using Eq. (7). The results are presented in Figure 11, where the red solid line represents the experimental data, and the blue solid line represents the theoretical response of a linear viscous single-degree-of-freedom model:

$$x(t) = e^{-\xi \omega_n t} \left[x_0 \cos(\omega_d t) + \left(\frac{\dot{x_0} + \xi \omega_n x_0}{\omega_d} \right) \sin(\omega_d t) \right]$$
 (7)

Where:

- x(t) is the displacement as a function of time,
- x₀ is the initial displacement,
- \vec{x}_0 is the initial velocity,
- ξ is the damping ratio,
- ω_n is the undamped natural frequency,
- $\omega_d = \omega_n \sqrt{1 \xi^2}$ is the damped frequency

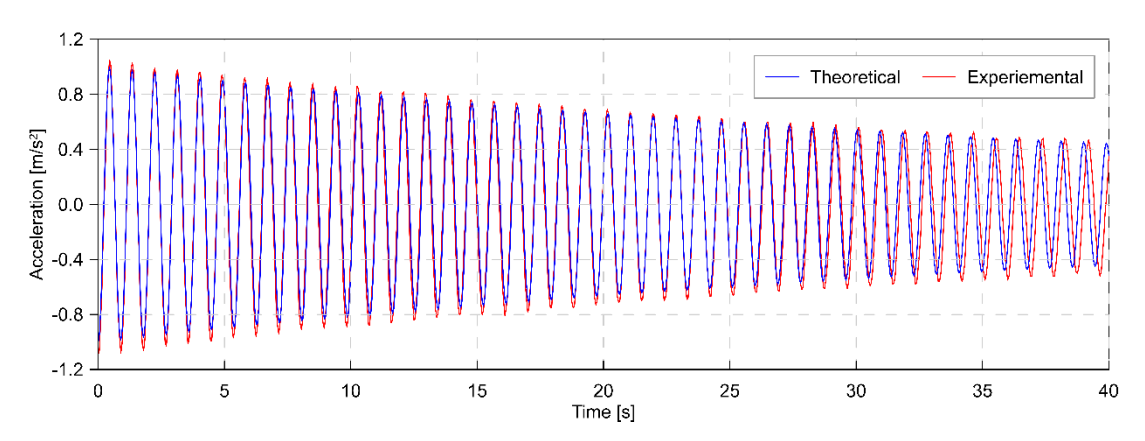


Figure 11. Comparison of experimental and theoretical acceleration responses of the structure without TMD over time



Figure 11 shows a notable correspondence between the theoretical and experimental curves, especially in the first 30 seconds, where the amplitudes of the oscillations coincide significantly.

By analyzing the time response, the natural frequency of the system (f_{n_exp}) was estimated through visual inspection, identifying the number of complete cycles observed within a specific time interval. It was determined that the experimental frequency of the system was $f_{n_exp} = 1.11 \, Hertz$, which is equal to the theoretical value calculated using Eq. (3).

Additionally, the experimental damping ratio (ξ_{exp}) was determined using the logarithmic decrement method, applying Eq. (8):

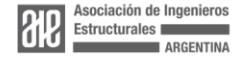
$$\xi_{exp} = \frac{1}{2\pi i} ln \left(\frac{x_n}{x_{n+1}} \right) \tag{8}$$

Where: x_n is the displacement peak in the n-th cycle,y x_{n+j} is the peak amplitude after j cycles, and j is the number of cycles considered.

To reduce measurement error and obtain a better estimate of the damping ratio, the first seven cycles of the structure's response were considered, yielding values of $x_n = 1.09 m/s2$ and $x_{n+j} = 0.96 m/s2$. Applying Eq. (8) with j=7, a damping ratio of $\xi_{exp} = 0.0029$ was obtained, corresponding to an experimental damping coefficient of $c_{s_exp} = 0.387 Ns/m$, which is very close to the target damping coefficient of $c_s = 0.388 Ns/m$.

Furthermore, the behavior of the combined system (primary structure-TMD) was evaluated, revealing a significant reduction in vibrations (See Figure 12). With values of $x_n = -0.75\,\mathrm{m/s^2}$ y $x_{n+J} = -0.4\,\mathrm{m/s^2}$ obtained from the figure for the structure with TMD over the first seven cycles, and applying Eq (8), it was determined that the implementation of the TMD increased the critical damping ratio of the structure from $\xi_{exp} = 0.0029$ without the TMD to $\xi_{exp_TMD} = 0.0143$ with the TMD. This increase in the critical damping ratio results in a significant reduction in vibrations, demonstrating the high effectiveness of the TMD in mitigating the dynamic response of the structure.

The high efficiency of the TMD can be attributed to two key factors. First, the primary structure without the TMD has a low initial damping ratio ($\xi_{exp}=0.0029$). In systems with reduced damping, the incorporation of a TMD significantly enhances the energy dissipation capacity, markedly improving the system's effective damping. Additionally, the TMD accounts for approximately 10% of the total mass of the primary structure. This substantial mass ratio allows the TMD to efficiently absorb and dissipate vibrational energy, reflected in the increased critical damping ratio.





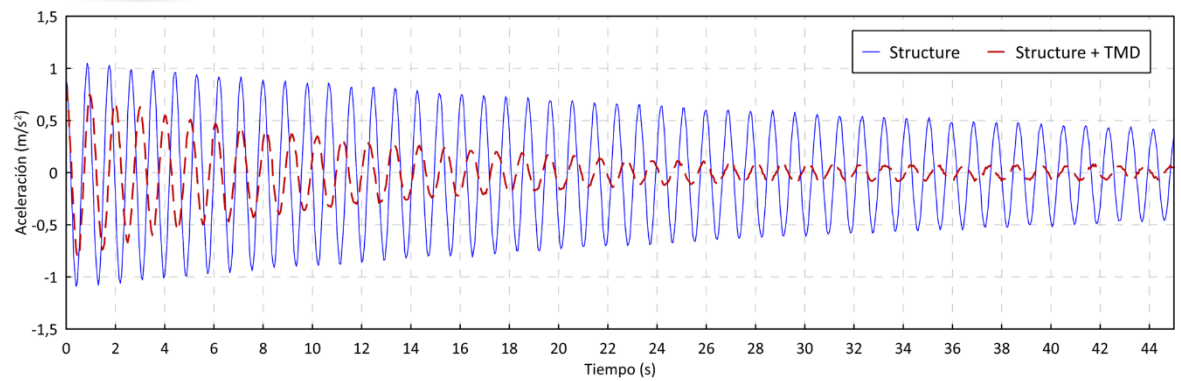


Figure 12. Comparison of acceleration responses of the structure with and without TMD.

The presented graphs demonstrate the effectiveness of the physical model in representing the dynamic behavior of the main structure. The good correspondence between the experimental data and theoretical predictions conclusively validates the accuracy of the model used.

It is important to note that the results shown in this section correspond to the first phase of an ongoing investigation. Although the results are promising, a detailed analysis of the TMD's dynamic behavior, including the effect of dry friction, will be addressed in later stages. Future studies will aim to determine to what extent dry friction may favorably or adversely influence the performance and efficiency of the TMD. These analyses are beyond the scope of this document, which primarily focuses on the fabrication process of the physical model.

CONCLUSIONS

This paper has presented the design and fabrication process of a physical model of a Tuned Mass Damper (TMD) mounted on a shear-frame structural model, with the objective of validating and approximating the dynamic response of the proposed theoretical model. A physical model has been successfully implemented throughout the work, allowing for the accurate estimation of the dynamic response of the multi-degree-of-freedom system under dynamic excitation conditions.

The results show that the primary structure, without the TMD, adequately reproduces the expected design parameters, including the natural frequency and critical damping ratio. This validation confirms that the physical model of the primary structure meets the design objectives. Additionally, the significant reduction in vibration amplitude observed when comparing the response of the structure with and without the TMD demonstrates the damper's effectiveness in vibration mitigation. Specifically, the implementation of the TMD increased the critical damping ratio of the structure from $\xi_{exp}=0.0029$ without the TMD to $\xi_{exp_TMD}=0.0143$ with the TMD. These initial results are consistent with the expected performance level of TMDs under ideal operating conditions.





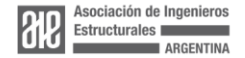
Although the focus of this document has been the design, fabrication, and assembly process of the physical model, a solid foundation has been established for future studies. These studies will focus on a detailed analysis of the TMD's dynamic behavior, including the influence of dry friction, to understand its impact on dynamic behavior and optimize its performance and efficiency.

ACKNOWLEDGEMENTS

We would like to express our sincere gratitude to the Vice-Rectorate for Research of the Universidad Técnica Particular de Loja (UTPL) for their invaluable support in the realization of this research. This piece of research has also been supported by the Catholic University of Córdoba, Argentina, and the Science and Technology Agency (SECyT) of the province of Córdoba. Their contributions have been fundamental to the success of this work, and their commitment to advancing knowledge is deeply appreciated.

REFERENCES

- Carmona, J. E. C., Avila, S. M., & Doz, G. (2017). Proposal of a tuned mass damper with friction damping to control excessive floor vibrations. *Engineering Structures*, *148*, 81–100. https://doi.org/10.1016/J.ENGSTRUCT.2017.06.022
- Dekemele, K., Van Torre, P., & Loccufier, M. (2020). Design, construction and experimental performance of a nonlinear energy sink in mitigating multi-modal vibrations. *Journal of Sound and Vibration*, 473, 115243. https://doi.org/10.1016/J.JSV.2020.115243
- Den Hartog, J. P. (1956). *Mechanical Vibrations, Fourth Edition* (4ta ed.). McGraw-Hill Book Company.
- Duque, E., Inaudi, J., & García, V. (2015). Efficiency of Tuned Mass Damper Attached To Structures With Elastoplastic Behavior and Subjected. *International Journal of Natural Disasters, Accidents and Civil Infrastructure*, *15*(1), 59–84.
- García, V. J., Duque, E. P., Inaudi, J. A., Márquez, C. O., Mera, J. D., & Rios, A. C. (2021). Pendulum tuned mass damper: optimization and performance assessment in structures with elastoplastic behavior. *Heliyon*, 7(6). https://doi.org/10.1016/j.heliyon.2021.e07221
- Jiang, J., Ho, S. C. M., Markle, N. J., Wang, N., & Song, G. (2019). Design and control performance of a frictional tuned mass damper with bearing–shaft assemblies. *Journal of Vibration and Control*, 25(12), 1812–1822. https://doi.org/10.1177/1077546319832429
- Rana, R., & Soong, T. (1998). Parametric study and simplified design of tuned mass dampers. *Engineering Structures*, *20*(3), 193–204.





- Roffel, A. J., Lourenco, R., Narasimhan, S., & Yarusevych, S. (2010). Adaptive Compensation for Detuning in Pendulum Tuned Mass Dampers. *Journal of Structural Engineering*, 137(2), 242–251. https://doi.org/10.1061/(ASCE)ST.1943-541X.0000286
- Tsai, H.-C., & Lin, G.-C. (1993). Optimum tuned-mass dampers for minimizing steady-state response of support-excited and damped systems.
- Wang, J., Wang, B., Liu, Z., Zhang, C., & Li, H. (2020). Experimental and numerical studies of a novel asymmetric nonlinear mass damper for seismic response mitigation. *Structural Control and Health Monitoring*, *27*(4), e2513–e2513. https://doi.org/10.1002/STC.2513
- Wang, L., Nagarajaiah, S., Zhou, Y., & Shi, W. (2023). Experimental study on adaptive-passive tuned mass damper with variable stiffness for vertical humaninduced vibration control. *Engineering Structures*, 280, 115714. https://doi.org/https://doi.org/10.1016/j.engstruct.2023.115714
- Warburton, G. B. (1982). Optimum absorber parameters for various combinations of response and excitation parameters. *Earthquake Engineering & Structural Dynamics*, 10(3), 381–401.

